INTERNATIONAL JOURNAL FOR NUMERICAL METHODS IN FLUIDS, VOL. 27, 57–80 (1998)

# GENERAL PURPOSE VERSUS SPECIAL ALGORITHMS FOR HIGH-SPEED FLOWS WITH SHOCKS

B. V. K. SATYA SAI,[1]* O. C. ZIENKIEWICZ,[1] M. T. MANZARI,[1]
P. R. M. LYRA[2] AND K. MORGAN[1]

[1]*Institute for Numerical Methods in Engineering, University of Wales, Swansea SA2 8PP, U.K.*
[2]*Department of Engineering Mechanics, Federal University of Pernambuco, 50.740-530 Recife, Brazil*

## SUMMARY

In this paper we compare the performance of a new general algorithm developed recently in application to problems of high Mach number flows with the performance of specialised algorithms applicable only to such flows. It appears that the results for most examples compare well, the biggest difference occurring in that of high Mach number compression corner. © 1998 John Wiley & Sons, Ltd.

*Int. J. Numer. Meth. Fluids*, **27**: 57–80 (1998)

KEY WORDS: high speed flow; shock modelling; numerical method; computational fluid dynamics

## 1. INTRODUCTION

With the advent of powerful computers, numerical modelling of fluid flow problems has emerged as a viable alternative to both experimentation and analytical solutions. However, to make computer simulations more widely acceptable and reliable, there is a continuing demand for the development of solution algorithms which can deal with complex flow phenomena in two and three dimensions and offer a high degree of accuracy, robustness and versatility. Any general method in computational fluid dynamics (CFD) has to ideally possess the capabilities of simulating the main flow features such as the values of velocity, pressure and density and predicting the viscous tractions in the presence of complicated geometries. Thus CFD algorithms have to be able to deal with the Navier–Stokes equations which govern the conservation of mass, momentum and energy of a viscous, heat-conducting and time-dependent flow. A simpler approximation of this general flow situation is possible by making the assumption that significant viscous effects and conduction effects are present only near the surface of the body and that the bulk of the flow is predominantly inviscid. From Prandtl's boundary layer analysis this is a valid approximation for attached flows at high Reynolds numbers away from the vicinity of solid surfaces. We then arrive at the so-called Euler equations. This approximation introduces significant changes in mathematical formulation as the system of partial differential equations describing the inviscid flow model reduces from second- to first-degree.

*Correspondence to: B. V. K. Satya Sai, Institute for Numerical Methods in Engineering, University of Wales, Swansea SA28PP, U.K.
Contract grant sponsor: NASA; Contract grant number: NAGW/2127 (AMES 90-144).

CCC 0271–2091/98/010057–24 $17.50 *Received May 1996*

Thus the starting point for most of the numerical schemes for compressible flow simulation are the time-dependent Euler or Navier–Stokes equations written in a conservation form. The advantages of considering unsteady state equations are twofold. One is that the transient behaviour can be modelled and the other is that the time-stepping formulation can be used as a relaxation or iterative process of reaching the solution for non-linear steady state problems. Writing the equations in the conservation form and preserving this form in the discretization allows us to obtain the correct jump relations at discontinuities.[1]

The most general choice for the discretization of the fluid flow equations is the finite element method (FEM), with the finite volume method (FVM) and the finite difference method (FDM) being its particular and non-optimal forms. Even though the FDM is traditionally the most popular choice in view of its long history and simplicity of use on uniform meshes, it suffers from the disadvantage that it is not readily applicable to irregular meshes and has a lower accuracy. The FVM, on the other hand, is quite flexible and can readily be used on arbitrary meshes. Its greatest advantage is that in the integral form the conservation laws are directly discretized, which ensures that the basic quantities, namely mass, momentum and energy, are apparent at the discrete level, but this, limits its use to the lowest (linear) type of spatial approximation. However, the FEM is the most general discretization method and, of course, is equally conservative. Like the FVM, it can be applied to arbitrary meshes and complex geometries. Further, it has the ability to incorporate gradient-type boundary conditions naturally and the ability to adapt the discretization based on the error in the approximate solution by means of mesh refinement, mesh movement or increasing the order of interpolation functions. Thus the FEM plays a significant role in the present-day CFD scenario.

The early part of the history of CFD has been dominated by structured mesh methodologies in view of their straightforward implementation, limited bandwidth, ability to produce computer codes for multidimensional analysis and ease of interchange of information among various grids for multigrid strategies. However, in the last decade there has been evidence of a move from structured to unstructured methodologies. Unstructured grids can be produced much faster for complex geometries, though they present such disadvantages as large memory requirement and possibly increased computational costs. However, the ability of unstructured meshes to resolve very-small-scale flow features in complex domains and their suitability for adaptive refinement have attracted both the finite element and finite volume followers to the use and development of unstructured mesh methodologies. This has also been made possible by the developments achieved in unstructured mesh generation, adaptivity, multigrid acceleration procedures and, more recently, computer architecture features such as vectorization and parallelization.

In the subsequent sections we first present the governing equations for compressible viscous flows and then describe some of the unstructured finite element algorithms developed in the recent past at the Institute for Numerical Methods in Engineering, Swansea for high-speed flow simulations. More recently, significant effort has been expended in two different directions towards achieving this objective. A novel, general algorithm based on the characteristic Galerkin approach and operator splitting has been developed that is suitable for both incompressible and compressible flows. This has been shown to give good results for a variety of problems involving fully incompressible as well as subsonic and supersonic flows. Simultaneously, a class of special purpose schemes based on the 'flux difference splitting' or Godunov method[2] has been implemented to deal with transonic through supersonic to hypersonic flows and these are particularly suited to very-high-speed flows with strong shocks. We present a review of the above methodologies and then compare their performance for a few hypersonic inviscid and viscous flow problems.

 

## 2. ESSENTIAL SUMMARY OF EQUATIONS

The full system of Navier–Stokes equations in non-dimensional form (and in conservative form) can be represented as

$$\frac{\partial U}{\partial t}+\frac{\partial F_i}{\partial x_i}=\frac{\partial G_i}{\partial x_i}. \tag{1}$$

Here, in two dimensions,

$$U^{\mathrm{T}}=[\rho,\ \rho u_1,\ \rho u_2,\ \rho E] \tag{2}$$

is the independent variable vector, where $\rho$ is the density of the fluid, $u_1$ and $u_2$ are the velocity components in the $x$- and $y$-directions respectively and $E$ is the total energy of the fluid

$$F_i^{\mathrm{T}}=[\rho u_i,\ \rho u_1 u_i+\delta_{1i}p,\ \rho u_2 u_i+\delta_{2i}p,\ u_i(\rho H)] \tag{3}$$

is the convective flux vector, where $p$ is the pressure and $H=E+p/\rho$ is the enthalpy of the fluid

$$G_i^{\mathrm{T}}=\frac{1}{Re}\left[0,\ \tau_{1i},\ \tau_{2i},\ \frac{\mu}{Pr}\frac{\partial T}{\partial x_i}+\tau_{ij}u_j\right] \tag{4}$$

is the diffusive flux vector, where $Re$ is the Reynolds number of the flow, $Pr$ is the Prandtl number of the fluid, $T$ is the temperature, $\mu$ is the dynamic viscosity of the fluid and $\tau_{ij}$ are the shear stresses given by

$$\tau_{ij}=\mu\left(\frac{\partial u_i}{\partial x_j}+\frac{\partial u_j}{\partial x_i}\right)-\frac{2}{3}\mu\frac{\partial u_k}{\partial x_k}\delta_{ij}. \tag{5}$$

The constitutive gas law is

$$p=(\gamma-1)\rho(E-0{\cdot}5u_i^2). \tag{6}$$

Finally the speed of sound $c$ is related to $\rho$ and $p$ as

$$c^2=\gamma p/\rho. \tag{7}$$

## 3. FINITE ELEMENTS IN COMPRESSIBLE FLOW SIMULATION

Even though considerable success has been achieved with the FEM for elliptic and parabolic problems, it is only in the last 15 years that it has attracted the attention of CFD developers for solving hyperbolic and hyperbolic-dominated problems. As mentioned in Section 1, the ability of the FEM to handle large complex geometries and differential boundary conditions in a natural way and the ability to deal with unstructured meshes are amongst its advantages over the FDM. Further, the developments in mesh generation capabilities,[3–6] multigrid acceleration procedures[7–9] and strategies for adaptivity[5,10] have led to the present-day progress in CFD in which full aircraft simulation[11–14] has become a reality. This indeed was first achieved through FEM codes.

The standard Galerkin method (which is similar to central differencing in the FDM) provides best approximation when used for discretizing symmetric and self-adjoint operators but yields suboptimal approximation for strongly convective equations. This often results in numerical procedures that are not stable for practical meshes and time steps. These difficulties were first resolved by the introduction of the Petrov–Galerkin formulation wherein the approximating shape functions are modified in such a way that the contribution of each element is not assigned evenly to each of its nodes but is distributed by taking into account the direction of the flow. This finite element equivalent

 

of upwinding was first introduced by Christie *et al.*[15] and followed by others.[16–19] Generalization to multidimensions was first carried out in Reference 16 but presented some 'cross-wind diffusion'. This difficulty was overcome in somewhat different ways by Kelly *et al.*[20] and Hughes and Brooks.[21] However, these formulations were derived for steady state formulations and scalar equations and their application to unsteady state systems of equations is not obvious.

The Taylor–Galerkin family of finite element methods for time-dependent equations was first introduced by Donea.[22] This method is the finite element equivalent of the Lax–Wendroff method[23] successfully used in the FDM. When applied to a system of fluid mechanics equations, it yields reasonable results but suffers from the disadvantage of having to evaluate and store the Jacobian matrices $A_i$ every time step. This operation is quite time-consuming. The two-step Taylor–Galerkin method,[24] which can be considered the finite element equivalent of the two-step MacCormack scheme,[25] avoids this difficulty by introducing an intermediate step. This method, while achieving the same accuracy as the one-step Taylor–Galerkin method, is computationally faster (by approximately a factor of three for 2D applications). Further developments of the Taylor–Galerkin method were carried out by Hassan,[26] who used an explicit/implicit method. This makes use of the alternating direction implicit (ADI) algorithm near the solid surfaces with a structured mesh, while in the rest of the domain an explicit method with an unstructured mesh is utilized. Even though the Taylor–Galerkin method is systematic and easily generalizable to multidimensions, in its derivation there is no obvious explanation as to why the standard Galerkin procedure is used and indeed effective for spatial discretization.

The characteristic Galerkin method, first introduced by Löhner *et al.*[27] and in which the scalar convection equation is transformed to a co-ordinate system along the characteristics, is fully justified theoretically. This process makes the convection equation self-adjoint along the characteristics and thus justifies the use of the Galerkin method for spatial discretization. However, for a scalar convection–diffusion equation the Taylor–Galerkin and characteristic Galerkin methods are identical. This justifies the Taylor–Galerkin method only for scalar variables and its extension to the full fluid equations often results in poor performance. It also suffers from another drawback. For instance, the Taylor–Galerkin approximation with equal-order interpolation to the Euler or Navier–Stokes equations fails as the compressibility tends to zero. This not only limits its range of application to high-speed flows but also affects the quality of high-speed compressible solutions in low-velocity zones such as near stagnation points.

## 4. GENERAL ALGORITHM[28]

The search for a suitable remedy for the above-mentioned drawbacks has led to the development of a general purpose algorithm that is designed to use the optimality of the Galerkin method for self-adjoint equations and to be able to perform over a wide range of flow situations ranging from fully incompressible flows through subsonic flows to highly compressible flows.

The philosophy behind this approach is to return to a single characteristic speed (for which the procedures were proved) by means of a suitable operator-splitting procedure. The key to such a split lies in a fractional step method devised originally by Chorin[29] and subsequently used by others[30–32] in the incompressible flow context. This method starts by obtaining an approximate velocity field using the momentum equation with the pressure gradients omitted. This step is followed by solving for the unknown pressure on inserting the velocity approximation into the continuity equation. The final stage is the correction of the velocity vector using the computed pressure terms. This method thus essentially separates the pressure calculation into one involving a Laplacian form which is self-adjoint and only a single characteristic velocity is involved in the first stage.

 

When the transient form is used for steady state results, another benefit arises. When the steady state equations for incompressible flow are cast in terms of the primitive variables $u$ and $p$, it can be readily seen that the appearance of zero diagonal terms renders the system singular unless the number of velocity variables is greater than the number of pressure variables. This condition, also known as the Babuška–Brezzi condition, restricts the use of equal-order interpolation for $u$ and $p$. Introducing an operator split as described above provides the remedy to this problem. The discrete steady state equations do not have a zero diagonal term, but instead a term proportional to the time increment appears and this allows arbitrary and convenient interpolations to be used for $p$ and $u$. For instance, an equal-order interpolation is possible avoiding the difficulties frequently encountered in the use of such interpolation with the previously mentioned Taylor–Galerkin procedure. Thus the essential step of the new general algorithm is the realization that in each computational step the transport of a single scalar quantity occurs and the application of characteristic Galerkin for each of these equations is fully justified. References 33–35 mark the various stages involved in the development of the general algorithm which was finally available for the conservative form of variables with a split, characteristic Galerkin approach.[28]

This scheme has been successfully applied in its explicit form to various subsonic and supersonic flow problems[36] and in semi-implicit form to various laminar/turbulent incompressible flow problems.[37] With further refinements in the prescription of boundary conditions[38] the general algorithm is applied (in what can be considered to be the final form) in the present work to some high-speed viscous and inviscid flow problems and its performance compared with some of the special purpose schemes to be discussed in the next section.

Following is a brief description of the steps involved in the split, characteristic formulation of the above equations. Here the governing convection–diffusion equation is first transformed into a co-ordinate system along the characteristic trajectory. This renders the equation self-adjoint in the new co-ordinate system for which the standard Galerkin discretization is optimal. However, this introduces the inconvenience of a moving co-ordinate system. To avoid this difficulty, a local approximation can be used as suggested in Reference 27. We then follow the Chorin-type[29] operator splitting and proceed with the spatial discretization. The resulting approximation is valid for any scalar convected quantity even if it is one of the components of the velocity $u$ itself, as is the case with the momentum conservation equations. Details of the characteristic approximation, operator splitting and Galerkin discretization can be found in Reference 28, but the following are the important steps involved.

*Step 1*

Solve for an intermediate velocity $\Delta(\rho\tilde{u}_i)$:

$$\Delta(\rho\tilde{u}_i) = \Delta t\left(-\frac{\partial(\rho u_i u_j)}{\partial x_j} + \frac{1}{Re}\frac{\partial \tau_{ij}}{\partial x_j} + \frac{\Delta t}{2}u_k\frac{\partial^2}{\partial x_k \partial x_j}(u_j \rho u_i) + \frac{\Delta t}{2}u_k\frac{\partial^2}{\partial x_k \partial x_i}[(1-\theta_2)P]\right)^n, \tag{8}$$

using the characteristic Galerkin process, which introduces the term involving $\Delta t$.

*Step 2*

Solve for $\Delta\rho$ (or $\Delta P$ in incompressible flows):

$$\Delta\rho = -\Delta t\left(\frac{\partial(\rho u_i)^n}{\partial x_i} + \theta_1\frac{\partial \Delta(\rho\tilde{u}_i)}{\partial x_i} - \Delta t\theta_1\frac{\partial^2 P^{n+\theta_2}}{\partial x_i \partial x_i}\right). \tag{9}$$

This equation is self-adjoint and hence the Galerkin process is optimal.

 

*Step 3*

Correct the velocities:

$$\Delta(\rho u_i)^{n+1} = \Delta(\rho \tilde{u}_i) - \Delta t \frac{\partial P^{n+\theta_2}}{\partial x_i}. \tag{10}$$

*Step 4*

Calculate $\Delta(\rho E)$ as a transport quantity:

$$\Delta(\rho E) = -\Delta t \left[ \frac{\partial}{\partial x_i}(u_i \rho E) - \frac{\partial}{\partial x_i}\left(\frac{\mu}{Re\, Pr}\frac{\partial T}{\partial x_i}\right) + \frac{\partial}{\partial x_i}(u_i p) - \frac{\partial}{\partial x_i}\left(\frac{1}{Re}\tau_{ij} u_j\right) + \frac{\Delta t}{2} u_k \frac{\partial^2}{\partial x_k \partial x_k}[u_i(\rho H)] \right]^n. \tag{11}$$

The above algorithm can be used in a semi-implicit manner and indeed only in this form can fully incompressible flow problems (with $M = 0$) be solved. In this case the following typical values of $\theta_1$ and $\theta_2$ are taken:

$$\tfrac{1}{2} \leqslant \theta_1 \leqslant 1, \qquad \tfrac{1}{2} \leqslant \theta_2 \leqslant 1.$$

This requires the solution of a system of equations in step 2 for pressure (or density). For the case of nearly compressible and compressible flows an explicit form of (9) can be derived by taking $\theta_2 = 0$.

It should be further mentioned that the above scheme, which is second-order-accurate in space and time, requires some additional dissipation to deal with strong discontinuities. Two different methods have been used in the present work. The first of these is based on a pressure-switch-type artificial viscosity method and has been used in all the examples considered in this work. This method is described in some detail in the Appendix. The second is based on an anisotropic artificial diffusion method as described in Reference 28. The application of this method in the present work is confined to the case of supersonic flow past a cylinder. Its implementation for the other cases is currently being pursued.

## 5. SPECIAL PURPOSE SCHEMES BASED ON FLUX DIFFERENCE SPLITTING

In this section we consider the higher-order upwind schemes based on Godunov's approach[2] and developed in the context of the finite element method. At present, truly multidimensional upwind-based schemes are still in the research stage. However, it is possible to extend the standard 1D upwind methods based on Godunov's method[2] to design multidimensional schemes.

The basic Godunov method solves over each mesh interval a locally one-dimensional shock tube problem. This scheme introduces into the numerical discretization information from the exact, local, non-linear solutions of the Euler equations. In this method there are three steps involved. In step 1 a piecewise constant approximation of the solution over each cell is defined at time $t$. The spatial error from this approximation over the cell size $\Delta x$ will be of the order of $\Delta x$ and hence the resulting scheme will be first-order. In step 2 a local Riemann problem is solved at the cell interfaces. The exact solution of the Riemann problem is a unique function of the initial conditions and the ratio $x/t$, where $x$ is the distance along the cell. In step 3 a new piecewise constant approximation is obtained by averaging the state variables after a time step $\Delta t$. Since in the whole method only step 2 is the physical step and is independent of steps 1 and 3 which are projection steps, it is possible to replace the piecewise constant approximation by a linear variation, resulting in a second-order space-accurate scheme of Van Leer.[39]

 

The exact solution of the Riemann problem in step 2 involves the solution of a non-linear algebraic equation and is quite time-consuming. This has led to the development of some well-known approximate Riemann solvers such as those of Roe[40] and Osher and Soloman.[41] However, the second-order upwind schemes are still not totally free from oscillations near discontinuities. Certain conditions were found to be necessary for non-oscillatory properties of these schemes. These are monotonicity, a concept introduced by Godunov,[2] monotonicity preserving,[42] total variation diminishing (TVD) introduced by Harten[43,44] and local extremum diminishing (LED) introduced by Jameson.[45] The utilization of these concepts has led to the development of a class of second-order schemes called 'high-resolution schemes' that provide non-oscillatory solutions. Very recently, finite element implementation of some high-resolution schemes has been carried out by Lyra[46] based on the TVD concept and by Manzari[47] based on the monotone upstream-centred scheme for conservation laws (MUSCL). (See also References 48–50.) These two schemes, using an edge-based data structure, are among the first of the finite element methods to utilize physical information in the discretization and yield excellent results especially for hypersonic flows.

### 5.1. *MUSCL scheme*[47]

After applying the Galerkin approximation to the Navier–Stokes equations, the discretization of the inviscid fluxes requires special care. It was shown by Peraire and Peiró[14] that the contribution of the inviscid fluxes to the finite element approximation can be related to an actual flux defined as

$$\mathbf{F}_{II_S} = \tfrac{1}{2}(\mathbf{F}^j_I \mathscr{S}^j_{II_S} + \mathbf{F}^j_{I_S} \mathscr{S}^j_{II_S}) \tag{12}$$

for interior nodes. Here $\mathscr{S}^j_{II_S}$ is the component in the $j$-direction of a geometry-dependent unit vector computed for edge $II_S$.

To construct a practical numerical scheme, we invoke Roe's flux-difference-splitting method,[40] which replaces the actual flux by the consistent numerical flux

$$\mathscr{F}_{II_S} = \tfrac{1}{2}[\mathbf{F}^j_I \mathscr{S}^j_{II_S} + \mathbf{F}^j_{I_S} \mathscr{S}^j_{II_S} - |\mathbf{A}_{II_S}|(\mathbf{U}_{I_S} - \mathbf{U}_I)], \tag{13}$$

where the Jacobian matrix $\mathbf{A}_{II_S}$ is computed in the direction of $\mathbf{S}_{II_S} = (\mathscr{S}^1_{II_S},\ \mathscr{S}^2_{II_S})$ from the so-called Roe average values as

$$\mathbf{A}_{II_S} = \mathbf{A}(\mathbf{U}_I,\ \mathbf{U}_{I_S}) = \mathscr{S}^j_{II_S}\left(\frac{\mathrm{d}\mathbf{F}^j}{\mathrm{d}\mathbf{U}}\right)_{II_S}. \tag{14}$$

However, this leads to a first-order upwind scheme which is too dissipative. A high-resolution scheme can be devised by using the MUSCL concept. In the context of the MUSCL algorithm the numerical flux for the inviscid flux contributions is rewritten as

$$\mathscr{F}_{II_S} = \tfrac{1}{2}[\mathbf{F}^j(\mathbf{U}_L)\mathscr{S}^j_{II_S} + \mathbf{F}^j(\mathbf{U}_R)\mathscr{S}^j_{II_S} - |\mathbf{A}_{II_S}|(\mathbf{U}_R - \mathbf{U}_L)], \tag{15}$$

where $\mathbf{U}_R$ and $\mathbf{U}_L$ are the interface values of the conservative variables for edge $II_S$. The interface values of the primitive variables $Z$ are obtained according to

$$Z^L_{II_S} = Z_I + \tfrac{1}{2}\mathscr{I}(Z_{I_S} - Z_I, Z_I - Z_{I_L}), \qquad Z^R_{II_S} = Z_{I_S} - \tfrac{1}{2}\mathscr{I}(Z_{I_S} - Z_i, Z_{I_R} - Z_{I_S}), \tag{16}$$

where $\mathscr{I}$ represents the interpolation function. In this work a function proposed by Thomas[51] is used:

$$\mathscr{I}(x, y) = \frac{x(y^2 + 2\varepsilon^2) + y(2x^2 + \varepsilon^2)}{2x^2 - xy + 2y^2 + 3\varepsilon^2}. \tag{17}$$

Here $\varepsilon^2$ is a small constant. More details about this scheme can be found in Reference 47.

 

*5.2. Symmetric TVD scheme*[46]

A finite element TVD scheme may be obtained by adopting the numerical flux function corresponding to the TVD formulation of the 1D Lax–Wendroff scheme (LW/TVD)[52] as

$$\mathscr{F}_{II_S} = \tfrac{1}{2}\{(\mathbf{F}_I^j \mathscr{S}_{II_S}^j + \mathbf{F}_{I_S}^j \mathscr{S}_{II_S}^j) - \mathbf{R}_{II_S}[\lambda^*(\mathbf{\Lambda}_{II_S})^2 \hat{\mathbf{Q}}_{II_S} + |\mathbf{\Lambda}_{II_S}|(\Delta_{II_S}\mathbf{W} - \hat{\mathbf{Q}}_{II_S})]\}, \tag{18}$$

where $\lambda^* = \Delta t^S / L_S$, with $L_S$ denoting the length of edge $II_S$, $\Delta t^S$ the local time step and

$$\Delta_{II_S}\mathbf{W} = \mathbf{R}_{II_S}^{-1}\Delta_{II_S}\mathbf{U} = \mathbf{R}_{II_S}^{-1}(\mathbf{U}_{I_S} - \mathbf{U}_I). \tag{19}$$

Here $\mathbf{R}$ and $\mathbf{R}^{-1}$ denote the matrices whose columns are the right and left eigenvectors of the Jacobian matrix $\mathbf{A}$ respectively, $\mathbf{\Lambda}$ is the diagonal matrix which contains the eigenvalues of $\mathbf{A}$ and $\hat{\mathbf{Q}}_{II_S}$ is a vector of limited characteristic variations. The resulting scheme is a symmetric TVD scheme, as upwinding is introduced only in the presence of the limiter and in the direction of the vector $\mathbf{S}_{II_S}$. As in the case of the MUSCL scheme, the approximate Riemann solver of Roe[40] is employed to resolve the interface between the two different fluid states.

The limited variations $\hat{\mathbf{Q}}_{II_S}$ are computed by making use of a locally structured stencil. Component $l$ of the vector, $\hat{Q}_{II_S}$, is computed using the characteristic variables and is determined from either an upwind-biased stencil or a symmetric stencil. For example, for $\Lambda_{II_S}^k > 0$ the limiter is defined to be either

$$\hat{Q}_{II_S}^l = \text{minmod}[\Delta_{II_S}W^l,\ \beta\Delta_{I_LI}W^l] \tag{20}$$

or

$$\hat{Q}_{II_S}^l = \text{minmod}[\beta\Delta_{I_LI}W^l,\ \Delta_{II_S}W^l,\ \beta\Delta_{I_SI_R}W^l]. \tag{21}$$

In these expressions the superscript $l$ denotes the $l$th characteristic field and $\beta$ is a parameter which makes the limiter more compressive, with $1 \leqslant \beta \leqslant 2$ for fully explicit schemes. The minmod function returns the value zero if any of its arguments are of opposite sign and the smallest argument in absolute value if the arguments are all of the same sign.

As only steady state computations are of interest here, we drop the Lax–Wendroff term, as suggested by Yee,[52] from the numerical flux described in (18), i.e. $\lambda^*$ is set equal to zero. For a very comprehensive discussion on the development of high-resolution schemes in the finite element framework see Reference 46.

The standard Galerkin method is applied to the viscous fluxes in the same way as for the inviscid fluxes. The functional dependence of the viscous fluxes upon the gradients of the primitive variables makes their approximation more prone to error. The most accurate way of computing the viscous flux contributions is to apply finite element approximation to each term in its expansion separately. However, it was shown by Peraire *et al.*[53] that this is not necessary and, in the context of an edge-based data structure, an approximation similar to what is used for the inviscid fluxes works well also for the viscous fluxes. This simplification has a significant benefit in terms of CPU time and memory requirements.

## 6. COMPARISON EXERCISE

The following test cases have been used to judge the performance of the general scheme[28] against the special purpose schemes[46,47] in different flow situations, namely supersonic/hypersonic and inviscid/viscous. However, all the viscous flow analyses are confined to laminar flow problems only.

 

### *6.1. Inviscid supersonic flow past a cylinder*

The first of the test cases is the inviscid flow past a cylinder at Mach 3. This is a challenging test case in the sense of stability, as it involves the presence of sonic, stagnation and rarefaction zones. The mesh used is an adapted mesh obtained from an initial coarser mesh. Details of the initial mesh for this as well as other problems are available in Reference 46. The adapted mesh consists of 12,651 nodes and 24,979 linear triangular elements and is shown in Figure 1(a). The Mach contours are

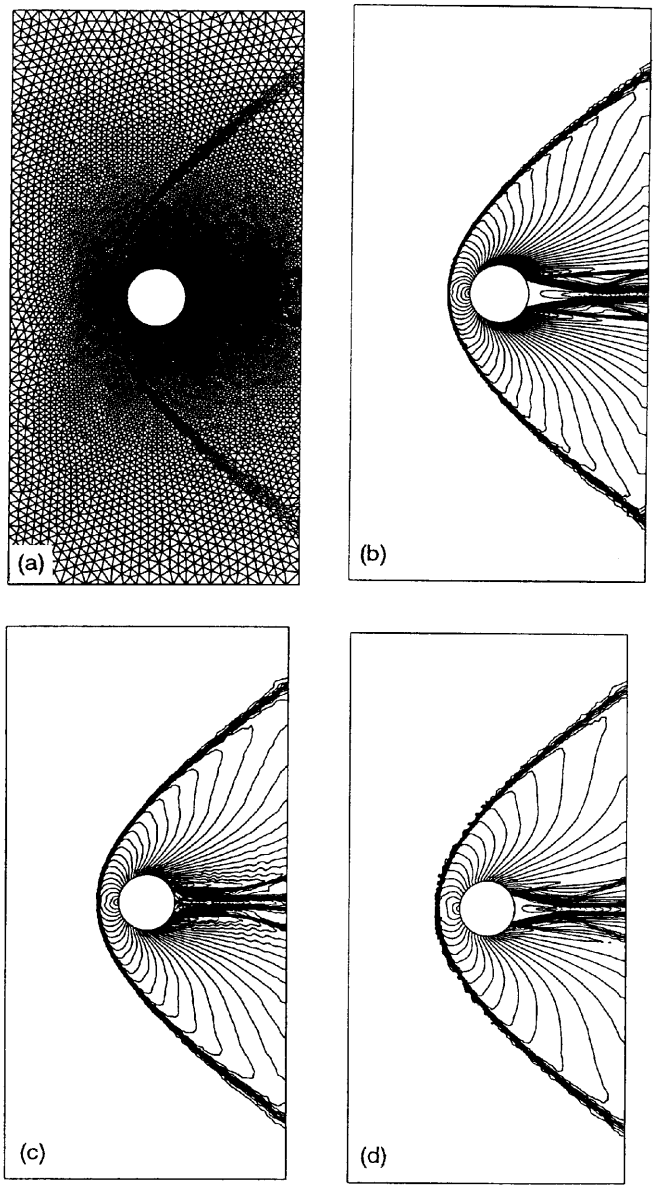


Figure 1. Inviscid flow past a cylinder, $M=3$: (a) adapted mesh (12,651 nodes 24,979 elements); (b) Mach contours with MUSCL; (c) Mash contours with general algorithm (pressure-switch-type artificial viscosity[64]); (d) Mach contours with general algorithm (anisotropic artificial viscosity[28])

 

presented for the MUSCL scheme in Figure 1(b). The Mach contours with the TVD scheme are very similar to those obtained with the MUSCL scheme and hence are not shown here. The Mach contours with the general scheme using the pressure-switch-type artificial viscosity are shown in Figure 1(c). Significant differences could be observed in the contours obtained with the general scheme and the MUSCL approach, especially in the quasi-rarefaction zone behind the cylinder where weak shocks are present. However, the bow shock in front of the cylinder appears to be represented by both methods in a similar fashion. To further study the performance of the general scheme, the anisotropic artificial diffusion method has been implemented for shock capturing and the resulting Mach contours are shown in Figure 1(d). These contours agree more closely with the MUSCL approach in the rarefaction zone than those with the pressure switch method. Based on these promising results,

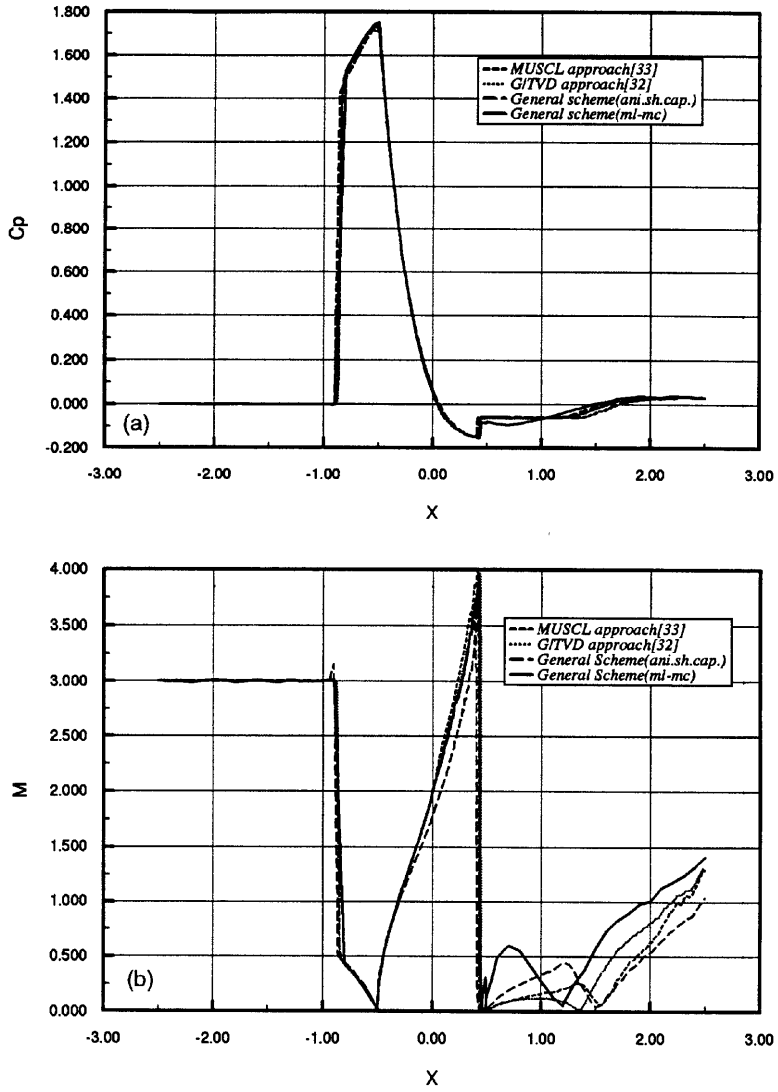


Figure 2. Inviscid flow past a cylinder, $M = 3$: comparison of (a) pressure coefficient and (b) Mach number variation along horizontal centre line and on cylinder surface

 

further work is currently in progress on its implementation. A comparison of the variation in coefficient of pressure and Mach number along the horizontal centre line of the geometry and on the surface of the cylinder is presented in Figures 2(a) and 2(b). There is very good agreement among the three schemes (i.e. MUSCL, G/TVD and the general scheme) with respect to $C_p$. From Figure 2(b) it can be observed that the sharp drop in Mach number through the bow shock in front of the cylinder, the acceleration over the cylinder wall and the subsequent drop in $M$ are captured equally well by all three methods. However, behind the cylinder there is disagreement among the three methods, with each method exhibiting different behaviour in the rarefaction zone.

The important considerations for this problem to produce a converged solution are the use of entropy correction and preventing the pressure from becoming negative behind the cylinder. While an entropy fix parameter is used in both the MUSCL and TVD schemes, no such parameter has been used in the general scheme. As a result the drop in the $L_2$-norm of the density residual is less for the general scheme by an order of $10^{-1}$–$10^{-2}$ as compared with the MUSCL and TVD schemes for all the problems considered in this work. Further, the reduction in the pressure to values very close to zero behind the cylinder leads to negative values during the initial stages of the transient behaviour. To prevent this from occurring, the procedure suggested by Thomas[51] is used with both the general and special purpose methods, which updates the thermodynamic variables according to the formula

$$\phi^{N+1} = \begin{cases} \phi^n + \Delta\phi & \text{if } \Delta\phi/\phi^n 0{\cdot}2, \\ \phi^n + \Delta\phi/[1]2(2 + |\Delta\phi/\phi^n|)] & \text{if } \delta\phi/\phi^n 0{\cdot}2. \end{cases} \tag{22}$$

### 6.2. *Shock interaction on a cylinder*

This problem involves the interaction of two inviscid transonic flows past a cylinder and hence is a more severe test case than the previous one. The mainstream Mach number is 15 and the disturbed stream Mach number is 10·596 at an angle of 6°. A schematic diagram of the flow and the geometry is shown in Figure 3(a). This represents a situation in which an oblique shock interacts with the bow shock in front of the cylinder. The initial mesh for this problem consists of 1703 nodes and 3217 elements. In order to resolve the interaction region properly, a very fine mesh is needed. The final mesh after four adaptations is used in the present work for comparison purposes. This consists of 7496 nodes and 14,693 linear triangles and is shown in Figure 3(b). The Mach contours with the MUSCL scheme and the general scheme are presented in Figures 4(a) and 4(b). Once again the Mach contours with the TVD scheme are not presented as they are almost identical with those of the MUSCL scheme. The shock in front of the cylinder is much thicker with the general scheme. This is due to the shock-capturing artificial viscosity used in the present example, namely equation (29) given in the Appendix. As mentioned in the Appendix, the pressure-switch-type artificial viscosity given by (30) has yielded a poor result and hence equation (29) has been used for shock capturing in this case. This expression, being proportional to $\Delta x^3$, spreads the shock over a greater number of elements. Figure 4(c) shows a comparison of the pressure on the surface of the cylinder in the $x_2$-direction. While the overall result is satisfactory, there appear some sharp oscillations especially where the shock impinges on the cylinder.

### 6.3. *Supersonic viscous flow past a flat plate*

This test case, originally solved by Carter,[54] is used to test the performance of the schemes for a viscous supersonic flow situation and requires the solution of the full Navier–Stokes equations. This problem consists of a Mach 3 flow over a flat plate at a Reynolds number of 1000 based on the length

 

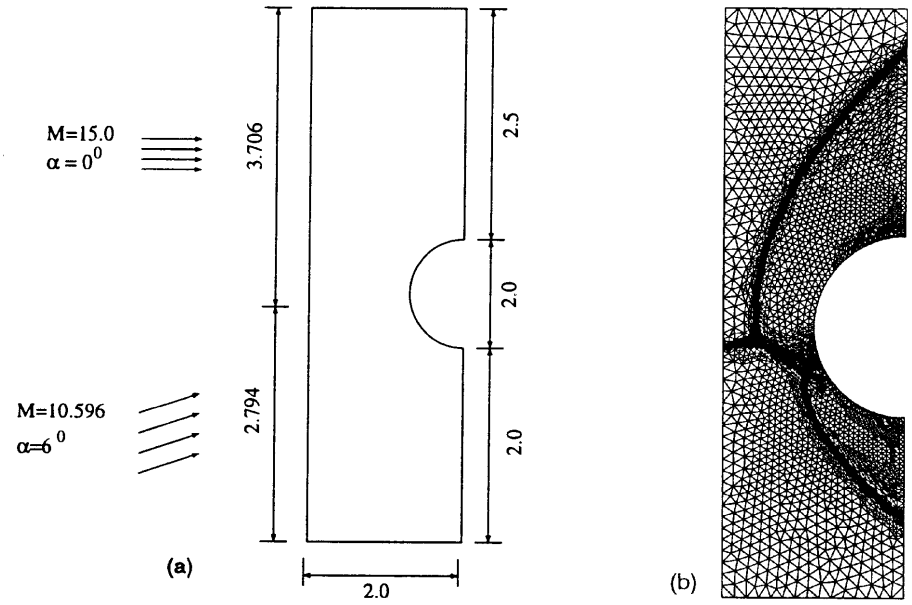


Figure 3. Inviscid shock interaction problem: (a) schematic diagram of flow domain; (b) fifth adapted mesh used in analysis (7496 nodes, 14,693 elements)

of the plate. The Prandtl number is taken as 0·72. The temperature of the plate is assumed constant and equal to the stagnation temperature $T_S$ defined as

$$T_S = \frac{1}{(\gamma - 1)M_\infty^2}\left(1 + \frac{\gamma - 1}{2}M_\infty^2\right), \quad \gamma = 1{\cdot}4. \tag{23}$$

The dynamic viscosity $\mu$ is assumed to vary with the temperature according to Sutherland's semiempirical equation

$$\frac{\mu}{\mu_r} = \frac{T + S_0}{T + S_0}\left(\frac{T}{T_r}\right)^{15}. \tag{24}$$

Figure 5(a) shows the structured mesh used in the analysis with 6750 nodes and 13,172 linear triangular elements. The mesh is graded in such a way as to have enough layers of nodes in the boundary layer. The first layer of nodes is located at a vertical distance of 0·0004$L$ from the plate, where $L$ is the length of the plate. This problem has been solved by the general scheme and the MUSCL approach. Figures 5(b) and 5(c) show the pressure contours and Mach contours with the general scheme, while those with the MUSCL scheme look similar and hence are not shown. Figures 6(a) and 6(b) show a comparison of the pressure along the plate and the $u_1$-velocity profile at the exit. The results of Carter[54] are also plotted. Barring a difference in the pressure distribution near the leading edge of the plate, there is overall agreement of the results between the general scheme and the MUSCL approach. It can be observed from the velocity profile that a more refined mesh is needed in the shock region where the velocity by the schemes varies less rapidly than Carter's.

 

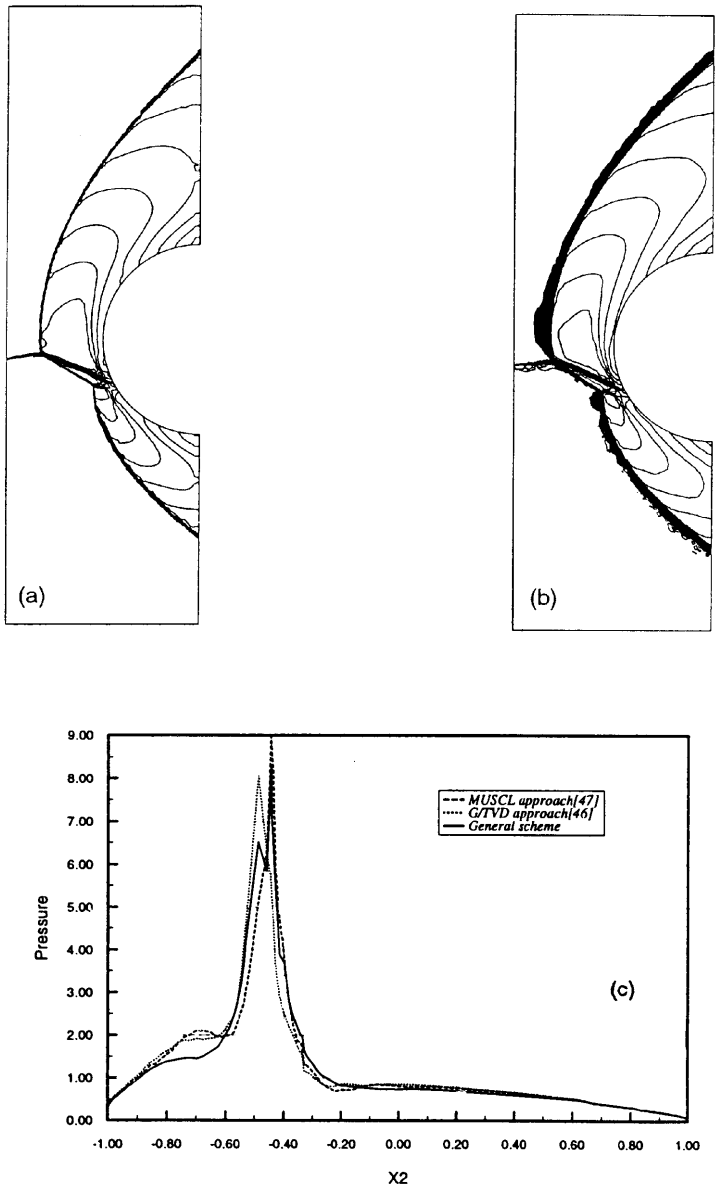


Figure 4. Results for inviscid shock interaction problem: (a) Mach contours with MUSCL; (b) Mach contours with general algorithm; (c) pressure distribution on cylinder in $x_2$-direction

### 6.4. *Hypersonic viscous flow past a flat plate*

The previous example deals with a supersonic flow situation at a somewhat low Reynolds number. The present example is a more severe test case and involves viscous flow past a flat plate at Mach 4 and a Reynolds number of $4 \times 10^6$ based on the length of the plate. The freestream temperature is fixed at 392·4 °R and the Prandtl number is 0·75. The flat plate is assumed to be adiabatic in this case. The severity of the problem requires that more nodes and elements be taken close to the solid wall

 

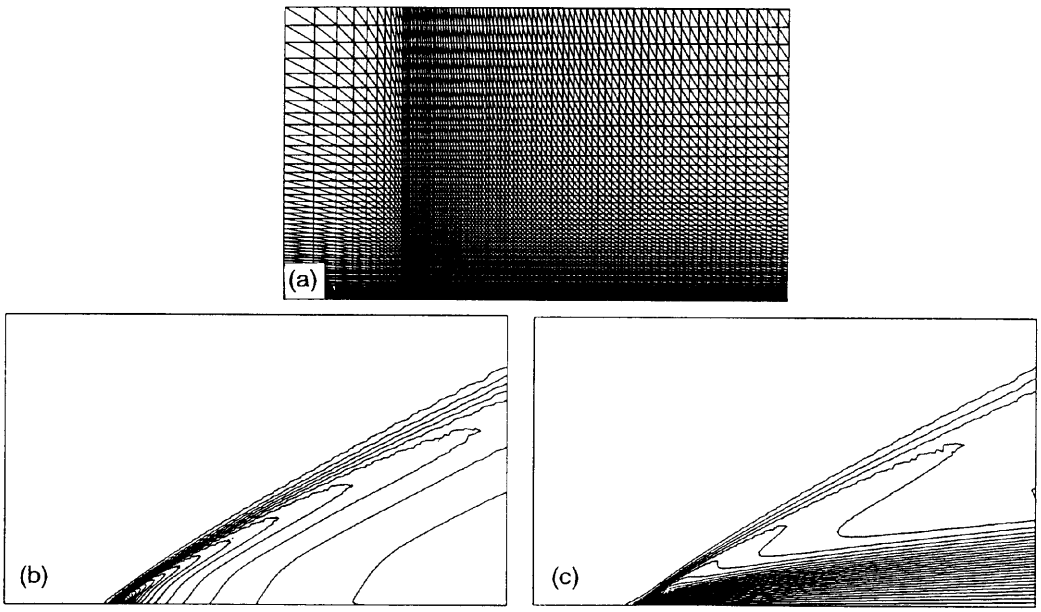


Figure 5. Viscous flow past a flat plate, $Re = 1000$, $M = 3$: The contours obtained by the general and special purpose schemes are identical (a) mesh used (6750 nodes, 13,172 elements); (b) pressure contours with general algorithm; (c) Mach contours with general algorithm

especially in the normal direction. As a result, highly stretched elements have to be used near the walls which rapidly reduce the speed of convergence to the steady state solution. The mesh used here is a structured grid with $101 \times 101$ nodes and 20,000 elements. The aspect ratio in the first layer above the wall increases from $0{\cdot}0001/0{\cdot}005 = 1/50$ at the leading edge to $0{\cdot}0001/0{\cdot}017525 = 1/175{\cdot}25$ at the trailing edge. The grid spacing in the normal direction changes in a graded manner. The mesh is shown in Figure 7(a). The most important issue in this example is the representation of the boundary layer, which can be gauged from the velocity profile at any section. A similarity solution for this case has been obtained by Van Driest[55] in terms of a non-dimensional variable

$$y^* = \frac{x_2}{x_1}\sqrt{(Re_{x_1})}, \tag{25}$$

where $Re_{x_1} = \rho_\infty U_\infty x_1/\mu_\infty$. Figure 7(b) shows a comparison of the non-dimensional velocity profile in terms of $y^*$ obtained by the general scheme, the MUSCL approach and the TVD approach at $x_1 = 0{\cdot}5$ The profiles at other sections are identical with the above. The similarity solution of Van Driest[55] is also plotted. It can be observed that for this example the general scheme slightly underpredicts the boundary layer thickness as compared with the other two schemes.

### *6.5. Hypersonic viscous flow over a compression corner*

The last of the viscous flow cases consists of a hypersonic flow over a compression corner of 24° angle. The freestream is at a Mach number of 14·1 and the Reynolds number is 103,680 based on a flat plate length of 1·44 ft. The temperature of the fluid in the freestream is 160 °R and the local Prandtl number is constant at a value of 0·72. The temperature of the wall is fixed at 535 °R. The Reynolds number is low enough to ensure that the flow is laminar and the free stream temperature is

 

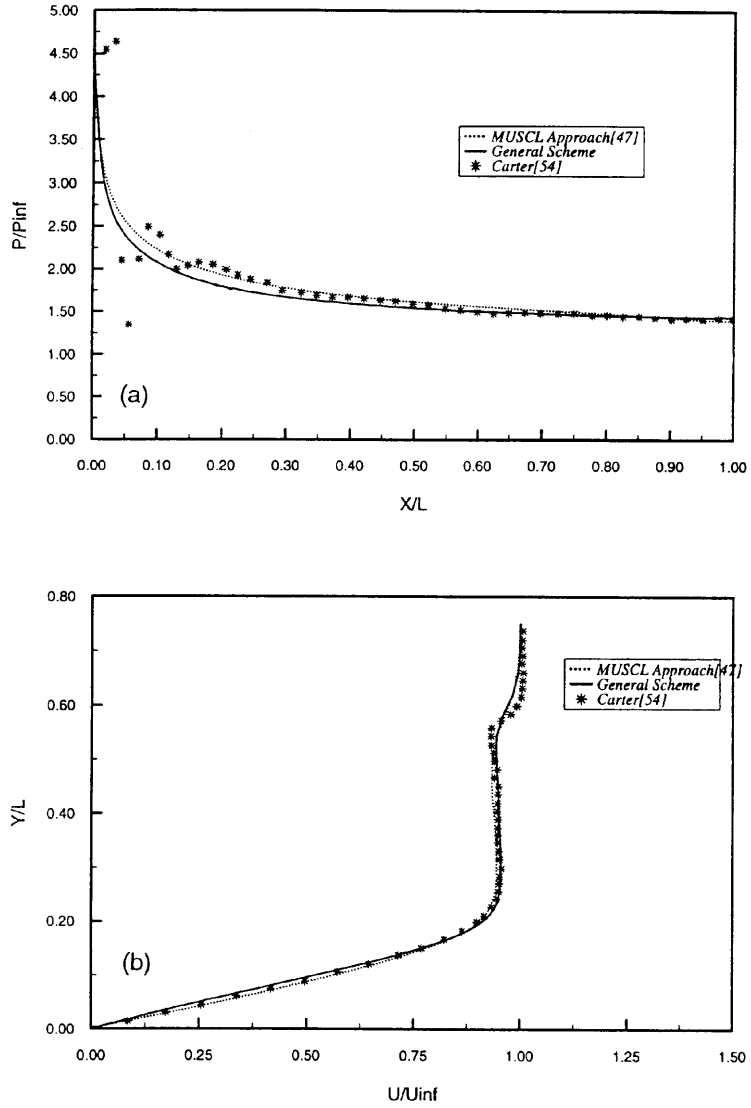


Figure 6. Comparison of results for Carter problem: (a) pressure distribution along plate; (b) velocity profile at exit section

low enough so that there are no significant real gas effects. The presence of a leading edge shock, a thin boundary layer on the ramp and shock–shock and shock–boundary layer interaction makes this problem computationally challenging for any numerical scheme designed to solve the Navier–Stokes equations. A schematic diagram of the problem with details of the flow behaviour is shown in Figure 8(a). The structured mesh with $111 \times 101$ nodes is shown in Figure 8(b). The $10 \times 101$ node extension of the mesh ahead of the flat plate was found to be necessary to remove oscillations close to the leading edge. Figures 9(a) and 9(b) show the pressure coefficient contours with the general scheme and the MUSCL approach respectively. Similarly, Figures 9(c) and 9(d) show the Mach contours obtained by the same. The corresponding plots with the TVD approach look very much like those by the MUSCL approach and hence are not presented here. Similarly to the shock interaction problem,

 

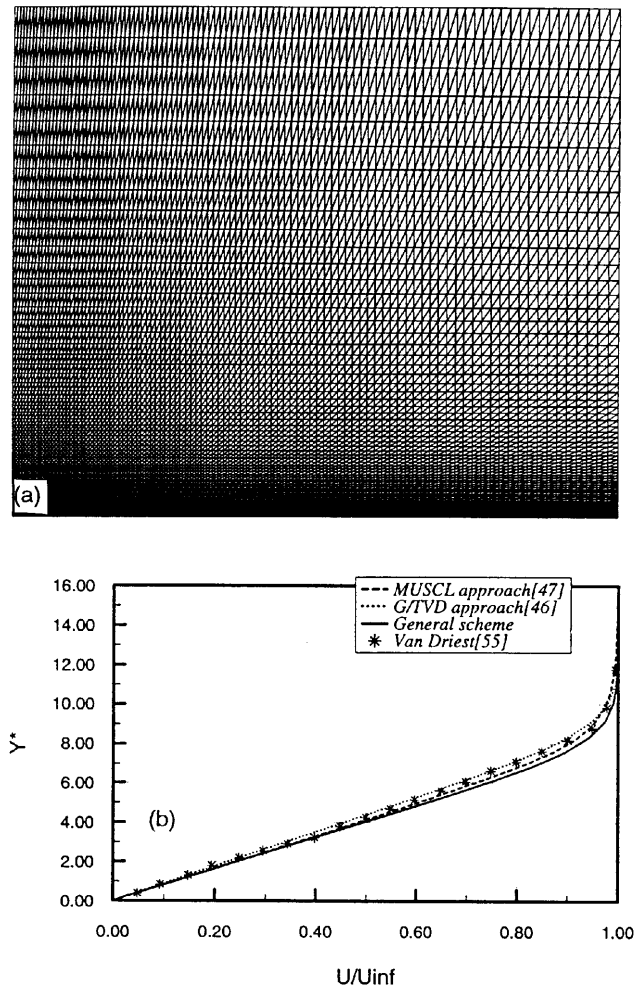


Figure 7. Hypersonic viscous flow past a flat plate, $Re = 4 \times 10^6$, $M = 4$: (a) mesh used (10,201 nodes, 20,000 elements); (b) comparison of velocity profiles with analytical solution at $x_1 = 0{\cdot}5$

in this case also the shocks are much thicker with the general scheme than the MUSCL scheme. This shows the inferiority of the shock capturing used with the general scheme. The best way to examine the solutions for this problem is to compare the wall coefficients $C_p$, $C_f$ and $C_h$. The following definitions are used in this work:

$$C_p = \log\left(\frac{50p_u}{\rho_\infty u_\infty^2/2}\right), \qquad C_f = 50\left(\frac{\tau_w}{\rho_\infty u_\infty^2/2}\right), \qquad C_h = \log\left(\frac{1000q_w}{\rho_\infty u_\infty (H_\infty H_w)}\right), \tag{26}$$

where the subscripts 'w' and '$\infty$' refer to the wall and the freestream conditions respectively. Here the wall shear stress and heat transfer rate are defined as

$$\tau_w = t_2^{(n)} n_1 - t_1^{(n)} n_2 = (\tau_{21} n_1 + \tau_{22} n_2) n_1 - (\tau_{11} n_1 + \tau_{12} n_2) n_2, \tag{27}$$

$$q_w = \partial T / \partial n = \nabla T \cdot \mathbf{n}, \tag{28}$$

 

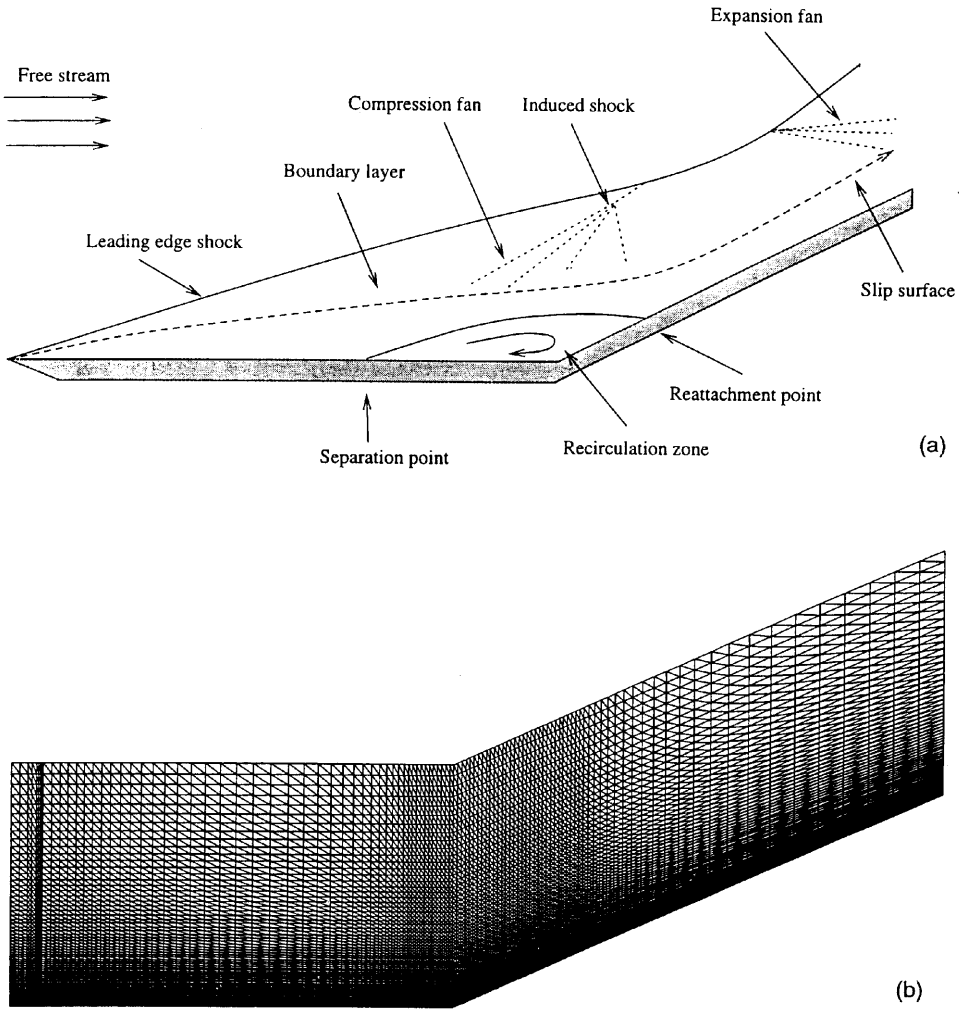


Figure 8. Hypersonic viscous flow over a 24° compression corner, $Re = 103{,}680$, $M = 14{\cdot}1$: (a) flow domain characteristics; (b) mesh used (11,211 nodes, 22,000 elements)

where $\mathbf{n} = (n_1, n_2)$ and $t_1^{(n)}$ and $t_2^{(2)}$ are the surface tractions in the direction $\mathbf{n}$. Figures 10(a)–10(c) show the pressure, skin friction and heat transfer coefficients obtained by the different methods. These plots also include the results obtained by Rudy *et al.*[56] using the structured mesh flow solver CFL3D. Significant differences can be observed between the general scheme and the rest of the schemes especially in regions close to the separation point and the point of peak pressure. From Figures 10(b) and 10(c) we observe that the general scheme underpredicts the skin friction and heat transfer coefficients near the reattachment point as compared with the MUSCL, TVD and CFL3D. A better shock-capturing scheme needs to be used with the general scheme to achieve better results, as any poor performance of the shock-capturing technique in the boundary layer or shock–boundary layer interaction region will adversely affect the solution.

 

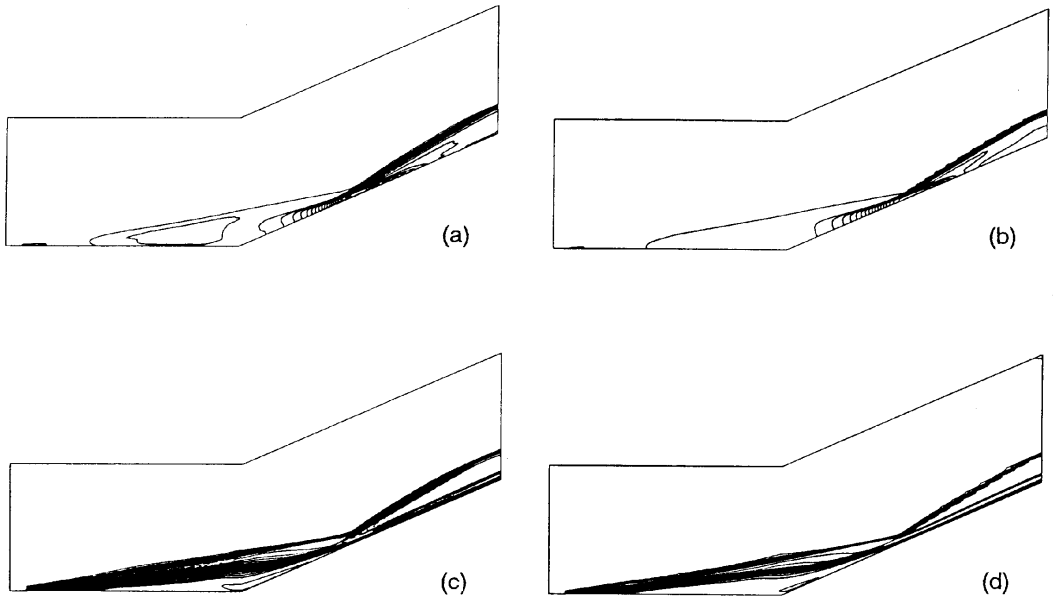


Figure 9. Comparison of (a, b) iso-$C_p$ and (c, d) iso-Mach contours with (a, c) general scheme and (b, d) MUSCL approach

## 7. CONCLUSIONS

In the present work we have made an effort to compare the performance of two different types of schemes designed to solve the Navier–Stokes equations for high-speed flows with shocks, via a number of examples. The first of these two classes of schemes is based on a general algorithm which has been recently introduced and proved to be suitable for a variety of problems ranging from fully incompressible through subsonic to supersonic flow situations. The second class of algorithms, based on the concepts of flux difference splitting and Riemann solvers, has been proved to yield good solutions for compressible flow problems in supersonic and hypersonic cases in particular. From the test cases presented here, which mostly deal with very-high-speed flows, it is observed that the performance of the general scheme is satisfactory on the whole and yields results comparable with those of the special purpose schemes. For hypersonic cases with Mach numbers as high as 14 the general scheme predictions deviate slightly from those obtained by the special purpose schemes. One possible explanation is that the general scheme needs to employ a more efficient shock-capturing technique that can produce sharp shocks. It is widely recognized that the ability of Riemann solvers to deal with shocks is superior to that of artificial viscosity schemes. Further, the TVD and MUSCL schemes employ tools such as entropy fixing which the general scheme does not specifically impose. This could have a significant effect on the convergence of the scheme. Thus for very-high-speed flows one would be inclined to favour the special purpose schemes. However, a bad performance of these schemes is possible when they are directly applied to nearly incompressible flows, in which region the general scheme performs well. The application of the anisotropic artificial diffusion method along with the general scheme seems to yield improved Mach contours for the case of an inviscid supersonic flow past a cylinder described in our first example and hence it could be considered worthwhile to apply this method to other examples considered in this work.

 

An important issue in this comparison is the computational cost. The TVD and MUSCL schemes use about twice as much computational time as the general scheme for each time step because of the Riemann solver. Thus the speed of computation is an advantage for the general scheme. Further, the extension of the general scheme to 3D is more straightforward than the extension of the TVD and MUSCL schemes to 3D. As mentioned earlier, truly multidimensional upwind methods on unstructured grids are still in the stage of development.

Finally, the fact that the general scheme, which performs well in the low-Mach-number range and indeed in the transonic range, can also achieve results close to those of specialized schemes as shown

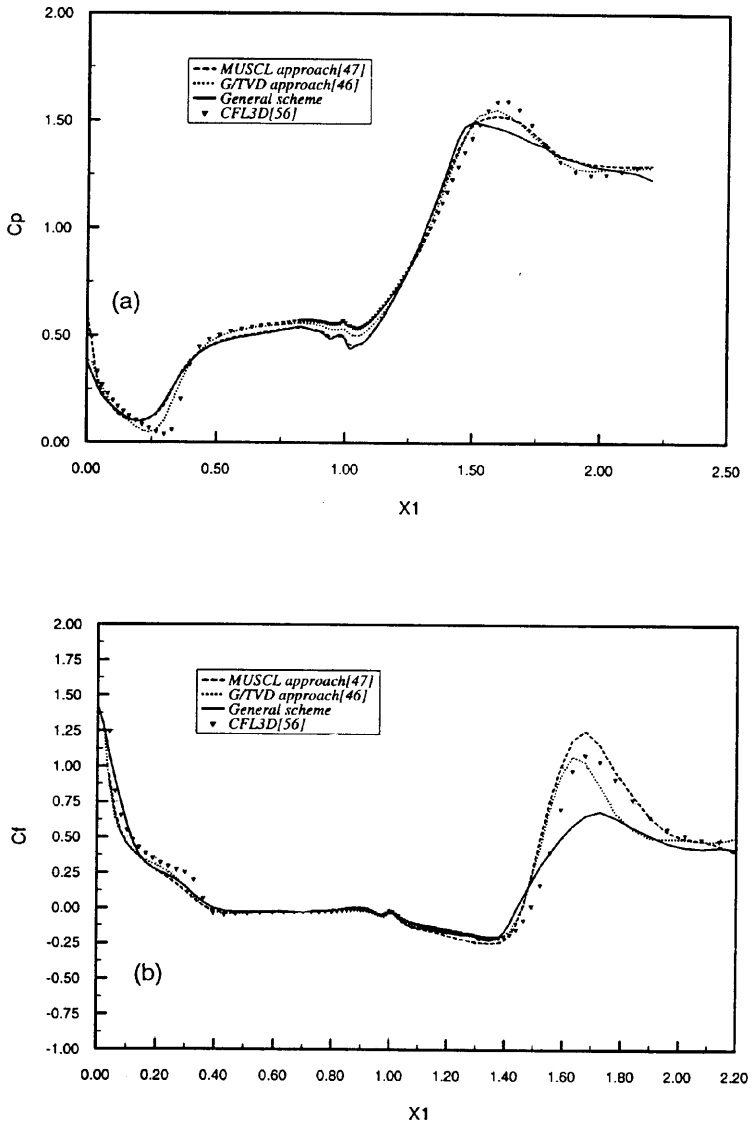


Figure 10. Hypersonic viscous flow past a compression corner: (a) coefficient comparison of pressure, (b) skin friction coefficient

 

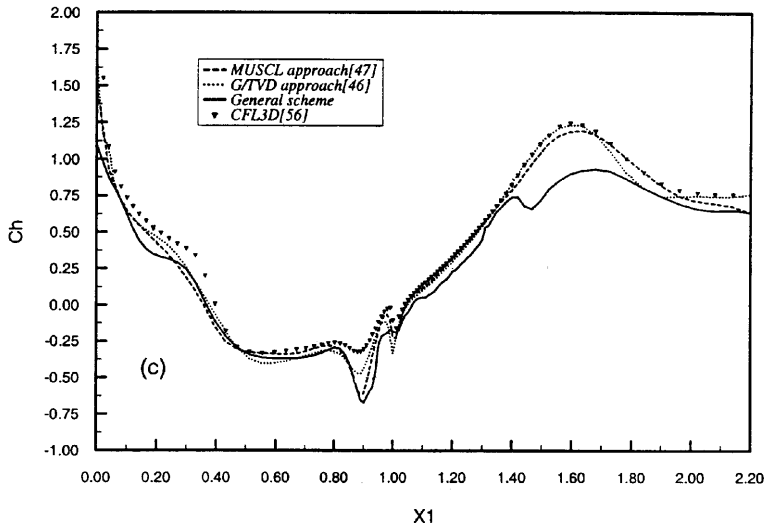


Figure 10. Hypersonic viscous flow past a compression corner: (c) heat transfer coefficient along wall

in this paper is remarkable. It therefore seems worthwhile to concentrate on more efficient shock-capturing techniques to extend its use and some such work is now in progress.

ACKNOWLEDGEMENTS

The authors are grateful to NASA, who, through grant NAGW/2127 (AMES 90-144), supported this research. The authors also acknowledge the help received from Dr. Nithiarasu Perumal, who carried out the computation with the anisotropic artificial diffusion method.

## APPENDIX

The most significant difference between the general purpose and special algorithms described earlier is the way in which discontinuities in flow are dealt with. Removing the high-frequency oscillations generated by the second-order schemes around discontinuities is of greatest importance in obtaining accurate numerical results for problems involving strong shocks. An extensive comparison of different approaches for treating the discontinuities and their relative merits and demerits are presented by Woodward and Collela.[57] In general, three major approaches are available: the artificial viscosity method, Godunov's approach and linear hybridization. While the general algorithm makes use of the artificial viscosity concept, the special purpose schemes are based on Godunov's approach for dealing with shocks.

The artificial viscosity method is the simplest of all the above. Originally suggested by von Neumann and Richtmeyer,[58] this method consists of representing the discontinuity as a narrow region of steep gradients in the flow variables. This is done by adding some artificial dissipation terms that mimic the action of viscosity in the neighbourhood of shocks. Other significant developments in this area are those of Lapidus,[59] McCormack and Baldwin,[60] Steger[61] and Jameson and co-workers.[62,63] Because these methods smear the discontinuities over three or more zones, fine grids are necessary to obtain narrow shocks.

 

The Godunov approach, which was discussed earlier, introduces explicit non-linearity into the discretization by approximating a hydrodynamic flow by a large number of constant states, computing their interactions exactly by using a Riemann solution and averaging the results in a conservative manner. While the advantage of this method is the accurate and well-behaved treatment of shock discontinuities, its main disadvantage is the complexity and the relatively larger amount of CPU time required as compared with the artificial viscosity method and the linear hybridization method.

Woodward and Collela's[57] investigation of the performance of the three approaches suggests that the Godunov method achieves the highest accuracy by means of elaborate calculations of the fluxes at zone interfaces near discontinuities. However, this complicates and slows down the scheme considerably. The artificial viscosity method is the simplest and fastest in terms of CPU time, but to achieve the same accuracy, the grid needs to be refined by at least a factor of two in each dimension and in time. However, considering the fact that the artificial viscosity method is much faster than the Godunov approach, it is still possible to achieve the same accuracy on a refined mesh in the same time.

While the implementation of Godunov's approach has been discussed in the special purpose schemes, the artificial viscosity method used in the general scheme is discussed below.

McCormack and Baldwin[60] suggested the following form of artificial viscosity for shock capturing:

$$\frac{\bar{U}_{\mathrm{s}}^{n+1} - \bar{U}^{n+1}}{\Delta t} = \frac{\partial}{\partial x_i}\left(\varepsilon \Delta x^3 \frac{|u| + c}{p}\left|\frac{\partial^2 p}{\partial x_i^2}\right| \frac{\partial \bar{U}^n}{\partial x_i}\right). \tag{29}$$

Here $\bar{U}^{n+1}$ is the solution at time step $n+1$, $\bar{U}_{\mathrm{s}}^{n+1}$ is the modified solution at time step $n+1$ after adding artificial viscosity and $\varepsilon$ is a user-defined factor (0·5–2·5). However, when applied to the FEM, the evaluation of $\partial^2 p/\partial x_i^2$ involves a variational recovery and could be expensive. Thus Peraire *et al.*[64] made the following modification based on some approximation:

$$M_{\mathrm{L}}\left(\frac{\bar{U}_s^{n+1} - \bar{U}^{n+1}}{\Delta t}\right) = \varepsilon \sum_{e=1}^{nel} \frac{S_e}{\Delta t_e}(M - M_{\mathrm{L}})\bar{U}^n. \tag{30}$$

$M$ and $M_{\mathrm{L}}$ are the consistent and lumped mass matrices respectively and $\bar{U}^n$ is the solution at time $n$. $S_e$ is an element pressure switch, which is the mean of the nodal values $S_i$, computed as

$$S_i = \frac{|\sum_k (p_i - p_k)|}{\sum_k |(p_i - p_k)|}. \tag{31}$$

$S_i = 1$ when the pressure has a local extremum at node $i$ and $S_i = 0$ when the pressure at node $i$ is an average of $p_k$. This form of artificial viscosity yields reasonably good shock properties for a wide range of problems but suffers from the disadvantage that $S_i$ could have non-zero values even in areas of smoothly varying pressure. This means that an additional diffusion is added even in the smooth flow regions which may not be very large for subsonic and supersonic cases. However, for hypersonic flow situations, because of the presence of very strong shocks, the amount of dissipation added would be more (a higher value of $\varepsilon$ is prescribed for high-Mach flows). This could seriously pollute the velocity and density fields and lead to a diffuse solution. This has been observed in the present exercise especially while solving the hypersonic flow problems. It has also been observed that the second gradient of pressure acts as a better switch than the switch described above. Thus switching over to the original artificial viscosity expression, namely equation (29) given by McCormack and Baldwin,[60] which uses the second gradient of pressure as a switch, has proved to be useful in obtaining meaningful results for the hypersonic flow cases. As the evaluation of $\partial^2 p/\partial x_i^2$ is expensive,

 

this form of artificial viscosity has been used only for the cases where the other one did not yield acceptable results. These cases are (i) shock interaction on a cylinder and (ii) hypersonic viscous flow over a compression corner. Another method towards which efforts are currently being directed is the anisotropic artificial diffusion method of Reference 28. Its implementation in the general scheme for the case of supersonic inviscid flow past a cylinder seems to provide improved Mach contours. Its application to other examples in the present work is currently being pursued.

## REFERENCES


1. P. D. Lax, 'Weak solutions of non linear hyperbolic equations and their numerical computation', *Commun. Pure Appl. Math*., **7**, 159–193 (1954).
2. S. K. Godunov, 'A difference scheme for numerical computation of discontinuous solution of hydrodynamic equations', *Math. Sb.*, **47**, 271–306 (1969) (in Russian; Engl. transl. *JPRS 7226*, 1969).
3. T. J. Baker, 'Generation of tetrahedral meshes around a complete aircraft', in T. J. Baker (ed.), *Numerical Grid Generation in Computational Fluid Dynamics*, Pineridge, Swansea, 1988, pp. 675-685.
4. O. Hassan, E. J. Probert, K. Morgan and J. Peraire, 'Linear relaxation methods for the solution of 2D and 3D compressible viscous flows using unstructured meshes', *Proc. Recent Developments and Applications in Aeronautical CFD*, Bristol, 1993.
5. J. Peraire, M. Vahdati, K. Morgan and O. C. Zienkiewicz, 'Adaptive remeshing for compressible flow computations', *J. Comput. Phys*., **72**, 449–466 (1987).
6. N. P. Weatherill, 'Mesh generation in computational fluid dynamics', *Tech. Rep. 1990–10*, Von Karman Institute for Fluid Dynamics, 1990.
7. R. Löhner and K. Morgan, 'Unstructured multigrid methods for elliptic problems', *Int. j. numer. methods fluids*, **24**, 101–115 (1986).
8. D. Mavriplis, 'Multigrid solution of two-dimensional Euler equations on unstructured triangular meshes', *AIAA J*., **26**, 824–831 (1988).
9. J. Peraire, J. Peiró and K. Morgan, 'Finite element multigrid solution of Euler flows past installed aero-engines', *Comput. Mech*., **11**, 433–451 (1993).
10. I. Babuška, O. C. Zienkiewicz, J. P. R. Gago and A. Oliveira (eds), *Accuracy Estimates and Adaptive Refinements in Finite Element Computations*, Wiley, New York, 1986.
11. A. Jameson, T. J. Baker and N. P. Weatherill, 'Calculation of inviscid transonic flow over complete aircraft', *AIAA Paper 86-0103*, 1986.
12. D. J. Mavriplis, 'Three dimensional unstructured multigrid for the Euler equations', *AIAA Paper 91-0721*, 1991.
13. K. Morgan, J. Peraire, J. Peiró and O. Hassan, 'The computation of three dimensional flows using unstructured grids, *Comput. Methods Appl. Mech. Eng*., **87**, 335–352 (1991).
14. J. Peraire and J. Peiró, 'A 3D finite element multigrid solver for the Euler equations', *AIAA Paper 92-0449*, 1992.
15. I. Christie, D. F. Griffiths, A. R. Mitchell and O. C. Zienkiewicz, 'Finite element methods for second order differential equations with significant first derivatives', *Int. j. numer. methods eng*., **10**, 1389–1396 (1976).
16. J. C. Heinrich, P. S. Huyakorn, O. C. Zienkiewicz and A. R. Mitchell, 'An ''upwind'' finite element scheme for two-dimensional convective transport equation', *Int. j. numer. methods eng*., **11**, 134–143 (1977).
17. T. J. R. Hughes and J. Atkinson, 'a variational basis for upwind finite elements', *Proc. IUTAM Symp*. Evanston, IL, 1978.
18. T. J. R. Hughes, 'A simple scheme for developing upwind finite elements', *Int. j. numer. methods eng*., **12**, 1359–1365 (1978).
19. T. J. R. Hughes and A. N. Brooks, 'A multidimensional upwind scheme with no crosswind diffusion', in T. J. R. Hughes (ed.), *Finite Elements for Convection Dominated Flows*, AMD Vol. 34, ASME, New York, 1979.
20. D. W. Kelly, S. Nakazawa, O. C. Zienkiewicz and J. C. Heinrich, 'A note on upwinding and anisotropic balancing dissipation in finite element approximations to convective diffusion problems, *Int. j. numer. methods eng*., **15**, 1705–1711 (1980).
21. T. J. R. Hughes and A. N. Brooks, 'A theoretical framework for Petrov Galerkin methods with discontinuous weighting functions; application to the streamline upwind procedure', in R. H. Gallagher, D. N. Norrie, J. T. Oden and O. C. Zienkiewicz (eds), *Finite Elements in Fluids*, pp. 47–66 Vol. 4, Wiley, New York, 1982.
22. J. Donea, 'A Taylor–Galerkin method for convective transport problems', *Int. j. numer. methods eng*. **20**, 101–119 (1984).
23. P. D. Lax and B. Wendroff, 'System of conservation laws', *Commun. Pure Appl. Math*., **13**, 217–237 (1960).
24. J. Peraire, 'A finite element method for convection dominated flows', *Ph.D. Thesis*, University of Wales, Swansea, 1986.
25. R. W. MacCormack, 'The effect of viscosity in hypervelocity impact cratering', *AIAA Paper 69-354*, 1969.
26. O. Hassan, 'Finite element computations of high speed viscous compressible flows', *Ph.D. Thesis*, University of Wales, Swansea, 1990.
27. R. Löhner, K. Morgan and O. C. Zienkiewicz, 'The solution of nonlinear system of hyperbolic equations by the finite element method', *Int. j. numer. methods fluids*, **4**., 1043–1063 (1984).


 

28. O. C. Zienkiewicz and R. Codina, 'A general algorithm for compressible and incompressible flow. Part I: The split, characteristic based scheme, *Int. j. numer. methods fluids*, **20**, 869–885 (1995).
29. A. J. Chorin, 'Numerical solution of the Navier–Stokes equations', *Math. Comput*., **23**, 341–354 (1968).
30. G. E. Schneider, G. D. Raithby and M. M. Yovanovich, 'Finite element analysis of incompressible fluid flow incorporating equal order pressure and velocity interpolation', in C. Taylor, K. Morgan and C. A. Brebbia (eds), *Numerical Methods in Laminar and Turbulent Flow*, Pentech, 1978.
31. M. Kawahara and K. Ohmiya, 'Finite element analysis of density flow using the velocity correction method', *Int. j. numer. methods fluids*, **5**, 308–323 (1985).
32. B. Ramaswamy, 'Finite element solution for advection and natural convection flows', *Comput. Fluids*, **16**, 349–388 (1988).
33. O. C. Zienkiewicz, 'Explicit (or semi-explicit) general algorithm for compressible and incompressible flows with equal finite element interpolation', *Chalmers University of Technology Rep. 90:5*, 1990.
34. O. C. Zienkiewicz, J. Szmelter and J. Peraire, 'Compressible and incompressible flow: an algorithm for all seasons', *Comput. Methods. Appl. Mech. Eng*., **78**, 105–121 (1990).
35. O. C. Zienkiewicz and J. Wu, 'A general explicit or semi-explicit algorithm for compressible or incompressible flows', *Int. j. numer. methods eng*., **35**, 457–479 (1992).
36. O. C. Zienkiewicz, K. Morgan, B. V. K. Satya Sai, R. Codina and M. Vazquez, 'A general algorithm for compressible and incompressible flow. Part II: Tests on the explicit form', *Int. j. numer. methods fluids*, **20**, 887–913 (1995).
37. O. C. Zienkiewicz, B. V. K. Satya Sai and K. Morgan, 'Split, characteristic based semi-implicit algorithm for laminar/ turbulent incompressible flows', *Int. j. numer. method. fluids*, **23**, 787–809 (1996).
38. R. Codina, M. Vázquez and O. C. Zienkiewicz, 'A fractional step method for compressible flows: boundary conditions and incompressible limit', *Proc. Int. Conf. on Finite Elements in Fluids—New Trends and Applications*, Venice, 1995, pp. 409–418.
39. B. Van Leer, 'Towards the ultimate conservative difference scheme. V: A second order sequel to Godunov's method', *J. Comput. Phys*., **32**, 101–136 (1979).
40. P. L. Roe, 'Approximate Riemann solvers, parameter vectors and difference schemes', *J. Comput. Phys*., **43**, 357–372 (1981).
41. S. Osher and F. Soloman, 'Upwind difference schemes for hyperbolic systems of conservation laws', *Math. Comput*., **38**, 339–374 (1982).
42. B. Van Leer, 'Towards the ultimate conservative difference scheme II. Monotonicity and conservation combined in a second order scheme', *J. Comput. Phys*., **14**, 361–370 (1974).
43. A. Harten, 'High resolution schemes for hyperbolic conservation laws', *J. Comput. Phys*., **49**, 357–393 (1983).
44. A. Harten, 'On a class of high resolution total variation stable finite difference schemes', *SIAM J. Numer. Anal*., **21**, 1–23 (1984).
45. A. Jameson, 'Artificial diffusion, upwind biasing, limiters and their effects on accuracy and multigrid convergence in transonic and hypersonic flows', *AIAA Tech. Rep. 93–3359*, 1993.
46. P. R. M. Lyra, 'Unstructured grid adaptive algorithms for fluid dynamics and heat conduction', *Ph.D. Thesis*, University of Wales, Swansea, 1994.
47. M. T. Manzari, 'An unstructured grid finite element algorithm for compressible turbulent flow computations', *Ph.D. Thesis*, University of Wales, Swansea, 1996.
48. M. T. Manzari, P. R. M. Lyra, K. Morgan and J. Peraire, 'An unstructured grid FEM/MUSCL algorithm for the compressible Euler equations', *Proc. VIII Int. Conf. on Finite Elements in Fluids: New Trends and Applications*, Pineridge, Swansea, 1993, pp. 379–388.
49. P. R. M. Lyra, M. T. Manzari, K. Morgan, O. Hassan and J. Peraire, 'Upwind side-based unstructured grid algorithms for compressible viscous flow computations', *Int. J. Eng. Anal. Des*., **2**, 197–211 (1995).
50. P. R. M. Lyra, K. Morgan, J. Peraire and J. Peiró, 'TVD algorithms for the solution of the compressible Euler equations on unstructured meshes', *Int. j. numer. methods fluids*, **19**, 827–847 (1994).
51. J. L. Thomas, 'An implicit multigrid scheme for hypersonic strong-interaction flow-fields', *Proc. Fifth Copper Mountain Conf. on Multigrid Methods*, 1991.
52. H. C. Yee, 'Construction of explicit and implicit symmetric TVD schemes and their applications' *J. Comput. Phys*., **68**, 151–179 (1987).
53. J. Peraire, K. Morgan, M. Vahdati and J. Peiró, 'The construction and behaviour of some unstructured grid algorithms for compressible flows', *Proc. ICFD Conf. on Numerical Methods for Fluid Dynamics*, Oxford University Press, Oxford, 1994, pp. 221-229.
54. J. E. Carter, 'Numerical solutions of the Navier–Stokes equations for the supersonic laminar flow over a two-dimensional compression corner', *NASA TR-R-385*, 1972.
55. E. R. Van Driest, 'Investigation of laminar boundary layer in compressible fluids using the Crocco method', *NASA Tech. Rep. 2597*., 1952
56. D. H. Rudy, J. L. Thomas, A. Kumar, S. R. Chakravarthy and P. A. Gnoffo, 'Computation of laminar hypersonic compression-corner flows', *AIAA J*., **29**, 1108–1113 (1991).
57. P. Woodward and P. Collela, 'The numerical simulation of two-dimensional fluid flow with strong shocks', *J. Comput. Phys*., **54**, 115–173 (1984).
58. J. Von Neumann and R. D. Richtmeyer, 'A method for the numerical calculations of hydrodynamical shocks', *J. Appl. Phys*., **21**, 232–237 (1950).
59. A. Lapidus, 'A detached shock calculation by second-order finite differences', *J. Comput. Phys*., **2**, 154–177 (1967).

 

60. R. W. MacCormack and B. S. Baldwin, 'A numerical method for solving the Navier–Stokes equations with application to shock-boundary layer interaction', *AIAA Paper 75-1*, 1975.
61. J. L. Steger, 'Implicit finite difference simulation of flow about two-dimensional geometries', *AIAA J.*, **16**, 679–686 (1977).
62. A. Jameson, W. Schmidt and E. Turkel, 'Numerical solution of the Euler equations by finite volume methods using Runge–Kutta time stepping schemes', *AIAA Paper 81-1259*, 1981.
63. A. Jameson and W. Schmidt, 'Some recent developments in numerical methods for transonic flows', *Comput. Methods Appl. Mech. Eng.*, **51**, 467–493 (1985).
64. J. Peraire, J. Peiro, L. Formaggia, K. Morgan and O. C. Zienkiewicz, 'Finite element Euler computations in three dimensions', *Int. j. numer. methods eng.*, **26**, 2135–2159 (1988).

 